Diffusion in Nickel Oxide Pellets—Effects of Sintering and Reduction

Diffusion rates were measured at 25°C and 1 atm by a steady state method in pellets of nonporous nickel oxide particles in order to determine the effects of sintering and chemical reduction. Sintering led to a striking decrease in diffusion flux; tortuosities above 100 were found for highly sintered (porosity 0.03) pellets. Reduction caused a sharp increase in diffusion rate when the original pellet was highly sintered. For an originally unsintered pellet the diffusion rate decreased with extent of reduction.

These phenomena were explained quantitatively by using: (1) the random pore model to predict tortuosity factors for an unsintered, unreduced pellet, and (2) the extent of pore interconnections and the fractional reduction to treat the effects of sintering and reduction. In this way an approximate, predictive equation was derived which contained no arbitrary parameters and which required for application only data on porosity and extent of chemical reduction.

K. K. KIM
and
J. M. SMITH

Department of Chemical Engineering
University of California
Davis, California

SCOPE

Sound technical design of equipment for gas-solid noncatalytic reactions, such as the reduction of pellets of metal ores, requires prediction of conversion vs. time curves as a function of reaction kinetics and the size and internal geometry of the pellets. The internal structure is important because the diffusion rate through the pores of the pellet can affect significantly the conversion-time relationship. For example, recent research on the reduction of nickel oxide pellets with carbon monoxide (Krasuk and Smith, 1972) and with hydrogen (Szekely and Evans, 1971) has shown that accurate values of the intrapellet diffusivities are necessary if reliable conversion vs. time results are to be predicted.

The significance of diffusion changes during the course of the reduction process due to changes in pore structure caused by sintering and by the chemical reaction itself. Optimum design would require a method of predicting how the diffusivity of the reducing gas is affected by these changes in structure. There appear to be no quantitative data and few theories in the literature on the effects of sintering and reaction on diffusion rates. The usual practice has been to assume that the diffusivity remains constant during the reduction. Calvelo and Cunningham (1970) improved the situation by supposing that the diffusivity is a function of porosity, as determined by the random pore model. This procedure, as the data in this paper show, may adequately account for the effect of porosity changes but does not account for the effects of other changes in pore structure during the reduction process. Szekely and Evans (1971) and Szekely et al. (1973) proposed an exponential decay in diffusivity with reaction time but made no attempt to relate the diffusivity to the changing pore geometry.

Our purpose was (1) to measure diffusivities in nickel oxide pellets as a function of extent of sintering and extent of chemical reduction, and (2) to develop a simple theory that would explain the diffusion data in terms of the changes that occur in the geometry of the pores. Of particular interest was the low porosity range where diffusion data were not found in the literature. The pellets were first prepared by compressing particles of non-porous nickel oxide and then these pellets were subjected to sintering and reduction operations.

CONCLUSIONS AND SIGNIFICANCE

From steady state diffusion measurements made for four binary gas systems He-N_2, He-CO_2 and CO-CO_2 at 25° to 200°C it was concluded that surface diffusion was negligible. The ratios of the diffusion fluxes and their temperature dependency showed that diffusion was of the Knudsen and bulk types in the pore volume of the pellets.

Sintering of unreduced pellets greatly reduced the diffusivity and the porosity; tortuosity factors greater than 100 were obtained for highly sintered (porosity = 0.03) pellets.

When highly sintered pellets were reduced, the diffusivity and porosity both increase due to the predominant effect of particle shrinkage. However, for unsintered pellets, reduction causes a decrease in diffusivity and an increase in porosity. Reduction is apparently accompanied by some sintering. Compression of unreduced, unsintered pellets to different porosities caused small reductions in diffusivity and porosity that were adequately correlated by the random pore model.

These diverse diffusion data could be explained by assuming that the primary influence of sintering was to decrease the pore interconnections and the effect of reduction was to change the porosity and the length of the diffusion path. The quantitative equations based upon this theory and on an isotropic pore structure accurately predicted diffusivities (tortuosity factors) down to porosities as low as 0.1. At lower porosities the effects of

Correspondence concerning this paper should be addressed to J. M. Smith.

anisotropy in the pore structure would have an unduly large effect and could explain the failure of the theory. Although the theory is a simplified one, it is believed adequate to demonstrate that pore interconnections and shrinkage are the predominant variables to use in explaining the effects of sintering and reduction on diffusion rates.

The Wicke-Kallenbach steady state method, (see experimental section), in which two gases diffuse in opposite directions through the pellet, was used to evaluate diffusion fluxes at atmospheric pressure. Measurements were made for four series of pellets. For each series, the pellets were prepared by changing the pore structure in a specific manner:

1. A series of sintered pellets in which the extent of sintering was changed by different heating times in an atmosphere of air (to prevent reduction) at 1250°C. The charge to the furnace consisted of unsintered, unreduced pellets. The porosity of the sintered pellets ranged from 0.44 to 0.03. Sintering reduced the size of the pellet but did not alter its shape.
2. A series of partially reduced (with hydrogen at 250°C), originally unsintered pellets. Extent of reduction was varied from 0 to 95% by the time of exposure to hydrogen. Reduction did not change the pellet size, but the porosity increased.
3. A series similar to the second except that highly sintered pellets were reduced.
4. A final series which consisted of unsintered, unreduced pellets prepared by using different pressures in pelleting the particles of NiO. For this series the porosity ranged from 0.44 to 0.57.

For these four series counter-diffusion rates were measured using the He-N_2 system at 25°C and atmospheric pressure. Prior to this, diffusion fluxes were measured for unsintered, unreduced pellets (#1 and 2) for four binary systems involving CO_2, CO, He, and N_2. All the results are shown in Table 1,* including experimental and theoretical (values in parentheses in Table 1) flux ratios calculated from the molecular weights by the expression:

$$\frac{N_B}{N_A} = -\sqrt{\frac{M_A}{M_B}} \tag{1}$$

This equation is approximately applicable for pore-volume diffusion in Knudsen or bulk transport regimes, but would not be valid if surface diffusion were significant. In all cases the experimental values agreed with the flux ratio calculated from Equation (1) within the accuracy of the experiments. The measurements for pellet #2 were for temperatures as high as 200°C. It was concluded that surface diffusion was not important for CO_2 or CO up to 200°C. For this reason the data for sintered and reduced pellets were obtained with the He-N_2 system.

An approximate effective diffusivity can be calculated by assuming that D_e is independent of concentration in the following equation for the diffusive flux

$$N_A = -\frac{P}{R_g T} D_e \frac{dy_A}{dz} \tag{2}$$

With D_e constant, integration for steady state conditions gives

$$N_A = \frac{P}{R_g T} D_e \frac{y_{A2} - y_{A1}}{z_2 - z_2} \tag{3}$$

where the subscripts 1 and 2 represent conditions on the end faces of the pellet. Since N_A, y_{A2}, and y_{A1} were measured, and the thickness of the pellet, $z_2 - z_1$, was known, D_e could be calculated. Results are shown in Figure 1 for pellet #2 and indicate from the slope of unity that D_e is about linearly dependent on the absolute temperature. Knudsen and bulk diffusivities are proportional to the

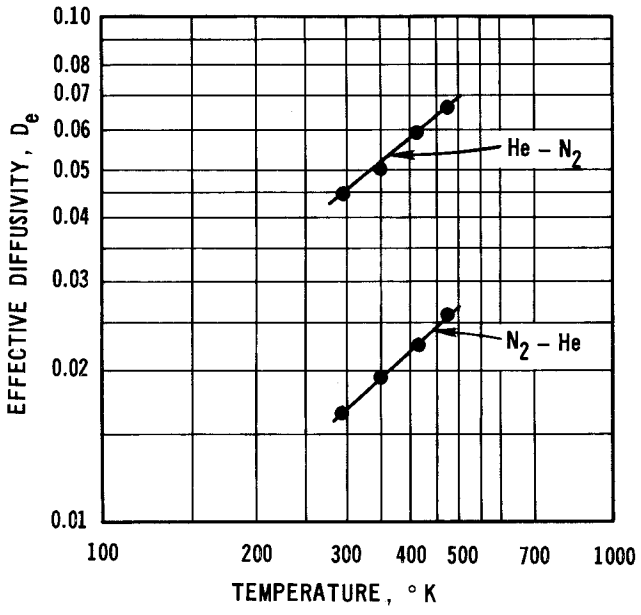

Fig. 1. Effect of temperature on effective diffusivities for unsintered, unreduced pellet (Pellet #2, $\epsilon = 0.44$).

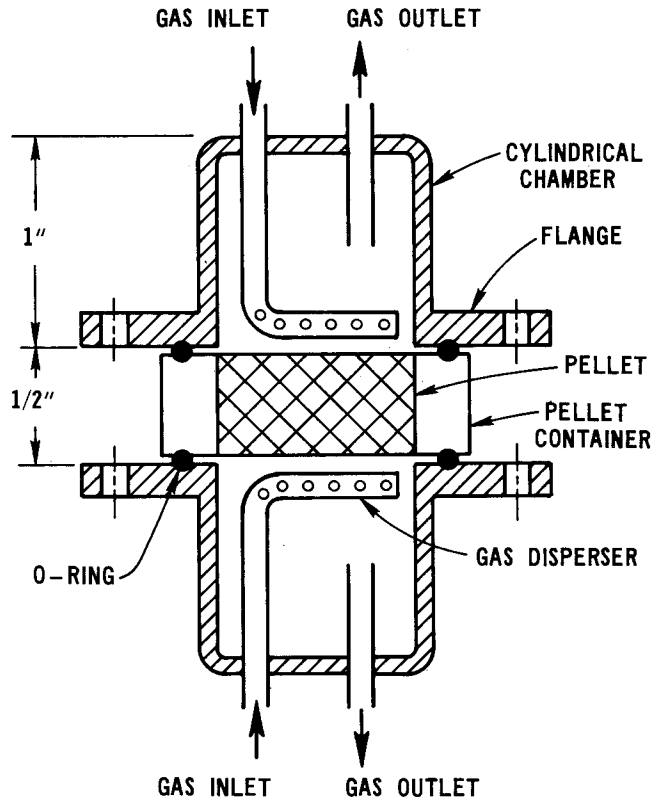

Fig. 2. Details of diffusion cell.

* Table 1 and supplementary material have been deposited as Document No. 02392 with the National Auxiliary Publications Service (NAPS), c/o Microfiche Publications, 305 E. 46 St., N. Y., N. Y. 10017 and may be obtained for $1.50 for microfiche or $5.00 for photocopies.

TABLE 2. PHYSICAL PROPERTIES OF PELLETS

Series	Condition	Pellet no.	Porosity	Pellet dimensions, cm Diameter	Length	Avg. pore radius, microns	Surface area, m^2/g
4	Unsintered	1	0.438	2.66	1.27	0.0402	6.1
	Unreduced	2	0.443	2.66	1.27	0.0412	6.0
		13	0.574	2.68	1.30	0.0700	5.4
1	Sintered	7	0.177	2.26	1.14	0.0505	0.99
	Unreduced	8	0.118	2.22	1.10	0.0553	0.60
		9	0.059	2.20	1.09	0.0462	0.39
		10	0.059	2.19	1.09	0.0290	0.25
		11	0.030	2.20	1.09	0.0460	0.37
		14	0.142	2.22	1.14	0.0460	0.37
		15	0.218	2.30	1.17	0.0560	2.90
		16	0.127	2.22	1.14	0.0460	0.95
2	Unsintered	18(0.345)[a]	0.530	2.66	1.26	0.090	3.3
	Reduced	19(0.955)[a]	0.660	2.66	1.29	0.200	2.3
3	Sintered[b]	20(0.953)[a]	0.439	2.20	1.08	0.155	0.72
	Reduced	21(0.300)[a]	0.194	2.20	1.08	0.096	1.2

[a] Number in parenthesis indicates fraction of NiO reduced to nickel.
[b] Sintered pellets before reduction had porosities of 0.09 and tortuosities of about 33.

one-half and three-halves power of the absolute temperature, respectively. Pore-size distribution measurements (see Figure 3) are such that Knudsen diffusivities are of the same magnitude as bulk diffusivities. Hence the diffusion in pellet #2 is in the transition region and a linear temperature dependency is, approximately, what would be expected. This relatively small effect of temperature is additional evidence that surface migration is not a contribution to the measured fluxes.

In addition to diffusion data, porosity and pore-size distribution measurements were made for all the pellets. This information was used to aid in evaluating the effects of sintering and reduction on pore structure and to determine the relative importance of Knudsen and bulk diffusion.

EXPERIMENT

The Wicke-Kallenbach apparatus (Figure 2) for constant-pressure, intrapellet diffusion measurements is well known (Wicke and Kallenbach, 1941) and consists of passing the two pure gases across opposite end faces of a cylindrical pellet. From analysis of the downstream gases and measurement of their flow rates, the counter-diffusion fluxes may be determined. Details of the apparatus and the care taken to obtain reproducible and accurate data, are described in the Supplement*. Standard methods were used to determine the porosity and pore size distributions of the pellets and these are also described in the Supplement.

Sintered pellets were prepared by heating the unreduced pellets in an electric furnace at 1250°C for 1 to 7 hours. Pellets were reduced in place in the diffusion cell by flowing hydrogen through the pores at 250°C. Detailed procedures are given in the Supplement.

RESULTS

Physical Properties

The size distribution of the NiO particles from which the pellets were made was determined by measuring 148 particles in a photograph at a magnification of 6000 times, obtained with a scanning electron microscope. The particles appeared to be nearly spherical in shape and to have diameters from 0.12 to 0.70 microns. The arithmetic average diameter was 0.45 microns.

The properties of the four series of pellets are summarized in Table 2. Pore volume distributions are given in Figure 3 for unreduced, unsintered (#1, 2, 13) and for unreduced, sintered (#7, 8, 9, 10, 16) pellets. The distributions are normalized with respect to total pore volume in order to eliminate the effect of the large reduc-

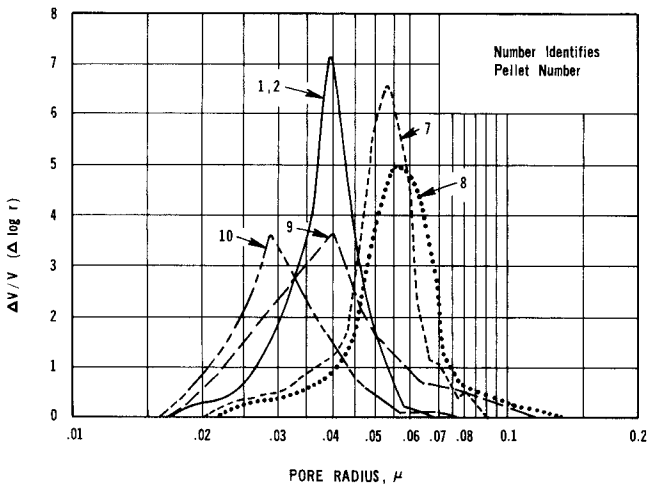

Fig. 3. Normalized pore size distribution for unsintered and sintered pellets.

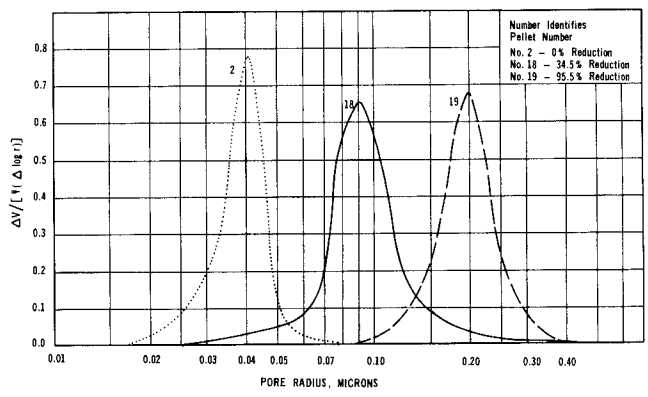

Fig. 4. Pore size distribution for reduced, unsintered pellets.

* See footnote on page 671.

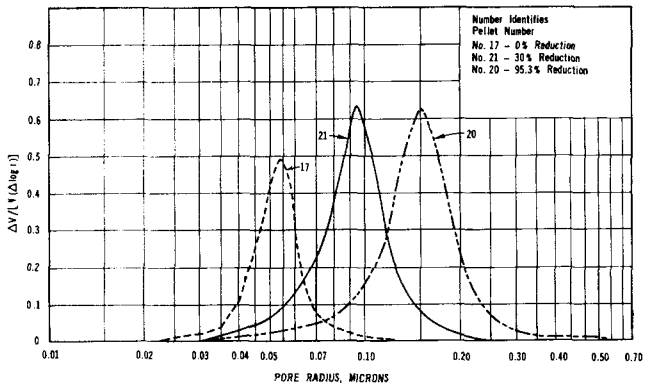

Fig. 5. Pore size distribution for reduced, sintered pellets.

tion in porosity accompanying sintering. These results indicate that in the early stages of sintering the volume of large pores grows somewhat at the expense of small pores, resulting in an increase in average pore radii. For highly sintered pellets (#9, 10) the small pores again increased slightly in number causing a decreasing in average pore radii. The effect of chemical reduction on the pore-volume distribution for the unsintered pellets is given in Figure 4 and for the sintered pellets in Figure 5. In both cases the average pore size increased significantly with reduction, corresponding to the observation that the pellet size was unchanged while NiO was converted to the more dense metallic nickel. The methods employed to calculate the average pore radii and the surface area, given in Table 2, are described in the Supplement*.

Diffusion Rates

Pellets #1 and #2 were prepared as duplicates, as closely as possible, in order to test the reproducibility of the data. The diffusion fluxes for these pellets shown in Table 1 for the same flow rates and for the same gas system indicate agreement within a few percent.

Diffusion data of the type obtained in this study are best analyzed in terms of tortuosity factors. This quantity is independent of gas system, temperature, and gas composition and should be a characteristic only of the pore structure, as far as diffusion is concerned. Tortuosity factors can be calculated from the measured fluxes in the following way. Equation (2), written for a straight, capillary, is

$$N_A = -\frac{P}{R_g T} D \frac{dy_A}{dz} \tag{7}$$

where D is a composite diffusivity. It has been shown for our case of constant pressure, counter diffusion (Evans et al., 1967) that D correctly accounts for Knudsen and bulk diffusion if it is expressed as

$$D = \frac{1}{\dfrac{1 - \alpha y_A}{D_{AB}} + \dfrac{1}{D_{KA}}} \tag{8}$$

The quantity α is determined by the flux ratio, which in turn can be expressed in terms of Equation (1):

$$\alpha = 1 + \frac{N_B}{N_A} = 1 - \left(\frac{M_A}{M_B}\right)^{1/2} \tag{9}$$

Note that D is a function of gas composition through y_A. Equation (7) may be applied approximately to porous media by introducing (and defining) a tortuosity factor δ

$$N_A = -\frac{P}{R_g T}\left(D \frac{\epsilon}{\delta}\right) \frac{dy_A}{dz} \tag{10}$$

The porosity is included in Equation (10) so that the flux N_A can be based upon the total of void plus solid cross-sectional area of the pellet. Substituting Equation (8) into (10), and integrating, gives

$$N_A = \frac{P}{\alpha R_g T}\left(\frac{\epsilon}{\delta}\right) \frac{D_{AB}}{z_2 - z_1} \ln\left(\frac{1 - \alpha y_{A_2} + D_{AB}/D_{KA}}{1 - \alpha y_{A_1} + D_{AB}/D_{KA}}\right) \tag{11}$$

Since steady state conditions exist in the pellet, N_A and α are constant, thus simplifying the integration. All quantities in Equation (11) except δ are known or measured. This expression was used to calculate tortuosity factors. Note that these results are not subject to the assumption of constant composition that is associated with the effective diffusivities evaluated from Equation (3). Also, δ defined by Equation (10), becomes a quantity characteristic of the pore structure; it is not a measure solely of diffusion path length but also includes such effects as pore shape and pore interconnections.

The variations in δ shown in Table 1 for different runs for the same pellet are the most appropriate overall measure of the accuracy of the data. Results for pellet #2 show that δ varies in a random way from 1.66 to 2.15 for four different gas systems over a temperature range from 25°C to 200°C, and for various flow rates.

The effects of sintering, shown by the experimental points in Figure 6, indicate an increase in tortuosity factor from about 2 (unsintered) to 100 (highly sintered). Also shown in this figure (pellets #1, 2, 13) are results for the effect of pelleting pressure (series 4). The key conclusion is that sintering causes a large decrease in diffusion flux.

Figure 7 shows the effects of reduction. For the initially highly-sintered pellet the tortuosity decreases sharply, and the porosity increases, with reduction. For the originally unsintered pellets, the opposite effect is observed: the tortuosity and porosity both increase mildly as reduction proceeds.

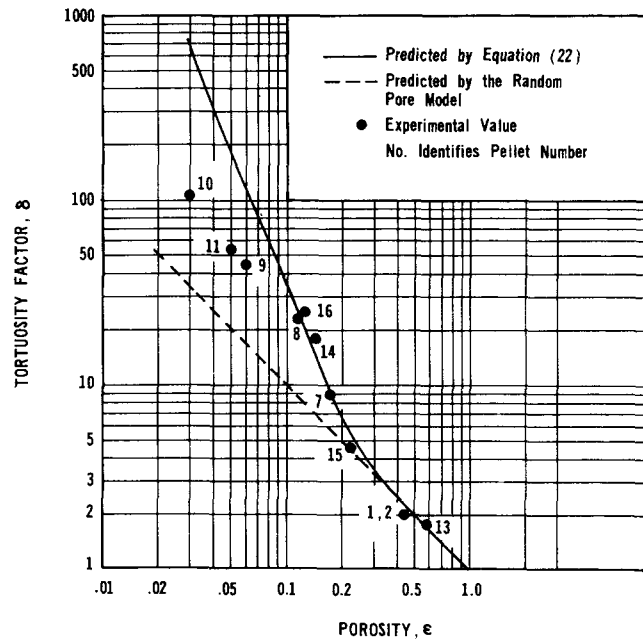

Fig. 6. Predicted and experimental toruosity factors for unreduced pellets ($\beta = 0$), both sintered and unsintered.

* See footnote on page 671.

THEORY

The random-pore model (RPM) developed (Wakao and Smith, 1962) for predicting diffusion rates through catalyst pellets is based upon a probability analysis of highly interconnected pores. The diffusion path length was taken equal to the minimum distance in the direction of diffusion. Hence, the tortuosity factor predicted by this model would be that associated with an assembly of highly interconnected pores. For a monodisperse porous medium containing only macropores, which describes the NiO pellets of this study, the RPM gives the following equation for the diffusion flux:

$$N_A = -\frac{P}{R_g T}(D\,\epsilon^2)\frac{dy_A}{dz} \qquad (12)$$

Comparison with Equation (10) shows that for the RPM

$$\delta = \frac{1}{\epsilon} \qquad (13)$$

This equation would be expected to fit the diffusion results for unsintered and unreduced pellets since this assembly of the NiO particles would provide for a maximum number of pore interconnections. The dotted line in Figure 6 corresponds to Equation (13) and does agree with the tortuosity factors observed for the unsintered, unreduced pellets 1, 2, and 13. Hence, the RPM is used as the basis upon which to add the effects of sintering and chemical reduction. Since the geometry of the pore structure is too complex to treat mathematically, simplifying assumptions are made. Therefore, the theory must be regarded as approximate. However, the theory does involve what are believed to be key variables and shows how they influence the tortuosity.

Effect of Pore Interconnections (Sintering)

The physical property changes accompanying sintering, for example, the decrease in porosity, suggest that pore interconnections are reduced as sintering occurs. The increase in tortuosity factors (decrease in diffusion fluxes) that results from sintering leads to positive deviations from the RPM, as seen in Figure 6. This also suggests that the alternate routes for diffusion, resulting in increased fluxes, are reduced as sintering occurs. Traditionally, the effect of sintering has been described in terms of pore closing and pore removal, as noted in various summaries (for example, Bonis and Hausner, 1964, and Kuczynski et al., 1967). Much of the published information is qualitative, and no attempt appears to have been made to analyze quantitatively the relation between sintering and diffusion. This paper attempts to do this by assuming that pore removal eliminates pore interconnections. Accordingly, a relationship is developed to describe the effect of pore interconnections on the diffusion flux, and hence, on δ.

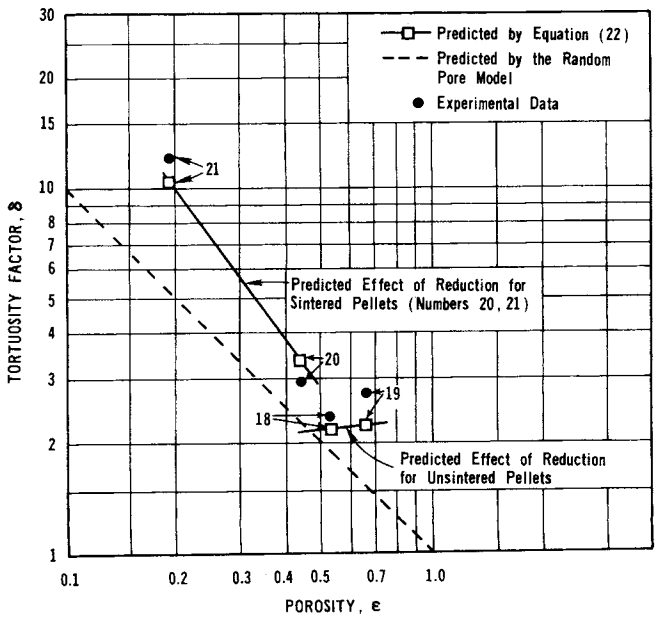

Fig. 7. Predicted and experimental tortuosity factors for reduced pellets ($\beta \neq 0$).

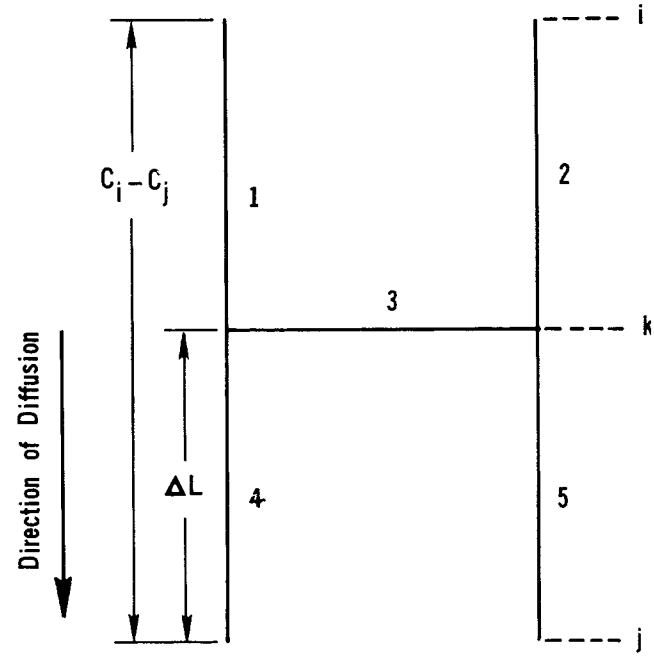

Fig. 8. 2 × 2 array of pores.

The pellet is supposed to consist of a number of identical arrays of pores. Hence, the tortuosity factor of the array will be equal to that for the pellet. The effect of pore interconnections is then evaluated by comparing diffusion fluxes through the array as individual pores are removed. As the number of pores removed increases, the number of calculations increase rapidly but they are all of the same, simple type.

The calculation procedure may be illustrated by considering a simple, but unrealistic, 2 × 2 array of five pores, as depicted in Figure 8. Each pore is regarded as a straight cylindrical tube of length ΔL. If the concentration drop across the array in the direction of diffusion is $C_i - C_j$ and N is the number of pores in the direction of diffusion, the flux through an array is, from Equation (10):

$$N_A = -\frac{P}{R_g T}\left(D\frac{\epsilon}{\delta}\right)\frac{dy_A}{dz} = \left(D\frac{\epsilon}{\delta}\right)\frac{C_i - C_j}{N(\Delta L)} \qquad (14)$$

This flux is based upon the total void plus nonvoid area perpendicular to the direction of diffusion. When no pores are removed from the 2 × 2 array, the actual void area will be $\epsilon/2$ since there are two pores. Since the pores are straight, the total flux through both pores is

$$N_A = D\left(\frac{\epsilon}{2}\right)\frac{C_i - C_j}{2(\Delta L)} + D\left(\frac{\epsilon}{2}\right)\frac{C_i - C_j}{2(\Delta L)}$$

$$= D\,\epsilon\frac{C_i - C_j}{2(\Delta L)}$$

Comparison of this result with Equation (14) shows that

$\delta = 1$ when no pores are removed and when there has been no reduction of NiO. If the fraction of pores removed is ϕ and the fraction of NiO reduced to Ni is β, we may write $\delta(\phi, \beta) = \delta(0, 0) = 1$.

If pore #1 (Figure 8) is removed the following flux equations may be written for the sections i to k (one pore) and k to j (two parallel pores):

$$N_A = D\left(\frac{\epsilon}{2}\right)\frac{C_i - C_k}{\Delta L}$$

$$N_A = D\left(\frac{\epsilon}{2}\right)\frac{C_k - C_j}{\Delta L} + D\left(\frac{\epsilon}{2}\right)\frac{C_k - C_j}{\Delta L}$$

$$= D\,\epsilon\,\frac{C_k - C_j}{\Delta L}$$

Eliminating C_k from these expressions gives

$$N_A = D\left(\frac{\epsilon}{1.5}\right)\frac{C_i - C_j}{2(\Delta L)}$$

The flux corresponding to removal, one at a time, of each of the other four pores can be evaluated in a similar way. If this is done, the average flux when one pore is removed is

$$(N_A)_{ave} = D\,\frac{\epsilon}{1.36}\,\frac{C_i - C_j}{2(\Delta L)}$$

This expression shows, by comparison with Equation (14), that $\delta(0.2, 0) = 1.36$. In an analogous way δ can be calculated for removal of 2, 3, and 4 pores, thus completing the evaluation for a 2×2 array. The variation in δ with individual pores introduces an uncertainty in the procedure. However, this variation is reduced as the total pores in the array are increased and is no more than 15% for the three-dimensional arrays.

Similar computations for three-dimensional arrays should provide a more realistic relation. For a $2 \times 3 \times 3$ array there are 30 pores (illustrated) in Figure 9), and the results are given in Figure 10. The function $g(\phi)$ represents the effect of pore interconnections and is defined

$$g(\phi) = \frac{\delta(\phi, 0)}{\delta(0, 0)} \qquad (15)$$

Computations for other three-dimensional arrays indicated relatively small variation with number of pores perpendicular to the direction of diffusion [see the curve for $2 \times 2 \times 2$ array in Figure (10)]. If the length of the pores is about the size of the particles used to prepare the pellets, no more than two pores should be necessary before the structure is repeated, indicating that either the $2 \times 2 \times 2$ or $2 \times 3 \times 3$ array would be satisfactory. The latter was chosen for final use since a wider range of tortuosity factors are possible for this array.

The objective was to develop a theory for predicting the tortuosity factor from easily measurable properties. Hence, the fraction of pores removed was determined from measured porosities. The quantity ϕ may be expressed as n/n_0, where n_0 is the total number of pores in the pellet and n is the number removed. For this porosity calculation it is assumed that the length and radius of all the pores are the same and that these dimensions do not change during sintering. Then the porosity is

$$\epsilon = \frac{\pi r^2(\Delta L)(n_0 - n)}{V_p} = \frac{\pi r^2(\Delta L) n_0}{V_p}\left(1 - \frac{n}{n_0}\right)$$

The porosity ϵ_0 of the unsintered, unreduced pellet is related to the pellet volume V_p by

$$\epsilon_0 = \pi r^2(\Delta L) n_0 / V_p$$

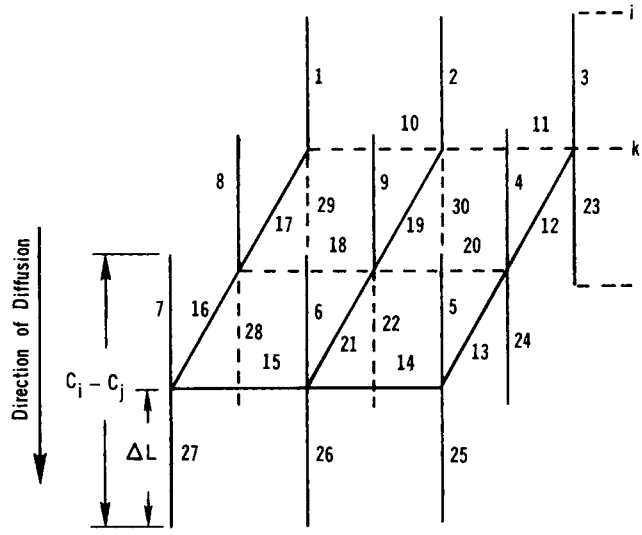

Fig. 9. $2 \times 3 \times 3$ array of pores.

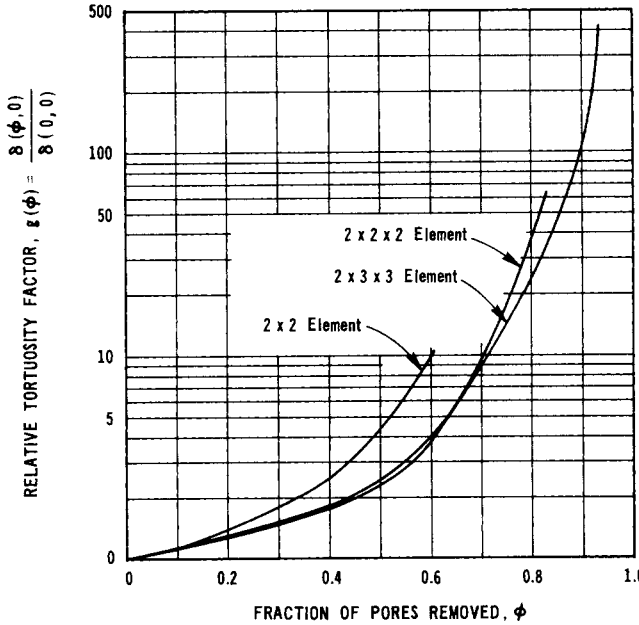

Fig. 10. Effect of pore interconnections on tortuosity factors.

These two expressions give

$$\epsilon = \epsilon_0(1 - \phi) \qquad (16)$$

As long as there is no chemical reduction, Equation (16) may be used to calculate ϕ from the measured porosity ϵ of the sintered pellet, and this ϕ then used with Figure 10 to determine the effect of sintering on δ; that is, to determine $g(\phi)$. Because of the assumptions involved, the linear relation suggested by Equation (16) must be regarded as an approximate one.

Effect of Chemical Reduction

During reduction the pellet size was constant but porosity increased. Presumably, this was due to the higher density of nickel with respect to that of NiO. The result was a shrinkage of the particles within the pellet and an increase in pore radii, as shown in Figures 4 and 5. This situation is described in an extreme way in Figure 11 where the unreduced particles of radius R_0 are in contact, but after reducing the smaller particles (radius R) are separated in such a way that the center-to-center distance

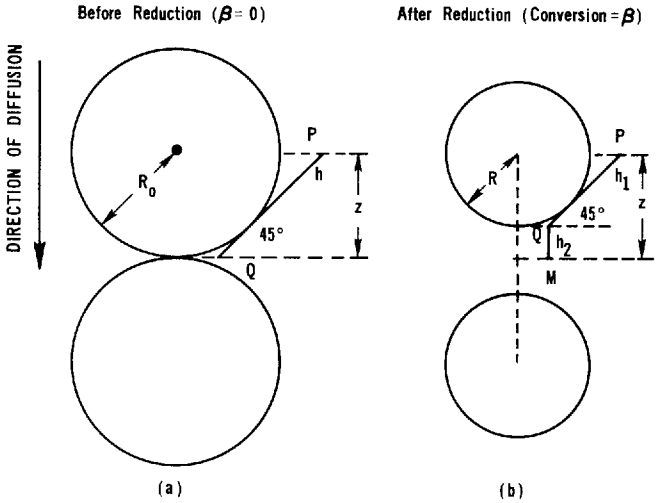

Fig. 11. Schematic representation of effect of reduction on tortuosity factor.

is unchanged. The effect of reduction on the tortuosity factor is supposed to be due to an increase in diffusion path length from h to $h_1 + h_2$, as indicated in Figure 11.

For the unreduced pellet the path is taken as the tangent line QP, making a 45° angle with the direction of diffusion. This leads to the traditional* tortuosity factor of $\sqrt{2}$; that is, for evaluating the effect of reduction, $\delta(0, 0) = \sqrt{2}$. For the reduced case QP is again tangent to the particle at an angle of 45°. Then the tortuosity factor is

$$\delta(0, \beta) = \frac{h_1 + h_2}{z} = (\sqrt{2} - 1)\frac{R}{R_0} + 1$$

The effect of reduction on δ is given by the ratio $\delta(0, \beta)/\delta(0, 0)$, or

$$\frac{\delta(0, \beta)}{\delta(0, 0)} = f(\beta) = \frac{1}{\sqrt{2}}(\sqrt{2} - 1)\frac{R}{R_0} + 1 \quad (17)$$

Next, it is necessary to express the ratio of reduced to unreduced particle radii R/R_0 in terms of the conversion. Also involved will be the densities of Ni and NiO and the porosity ϵ_{Ni} of the nickel layer formed around the NiO particles during the reaction

$$NiO(s) + H_2(g) \rightarrow Ni(s) + H_2O(g)$$

From reaction stoichiometry and straightforward geometry (Kim, 1973), the required relation is

$$\frac{R}{R_0} = \left[\frac{0.78\,\rho_{NiO}\beta}{\rho_{Ni}(1 - \epsilon_{Ni})} + 1 - \beta\right]^{1/3} \quad (18)$$

where 0.78 is the ratio of molecular weights of Ni and NiO.

Elimination of R/R_0 from Equation (17) using (18) gives the effect of reduction on the tortuosity factor, expressed in terms of β and other known quantities, except for ϵ_{Ni}. The result is

$$f(\beta) = \frac{1}{\sqrt{2}}\left\{(\sqrt{2} - 1)\left[\frac{0.78\,\rho_{NiO}\beta}{\rho_{Ni}(1 - \epsilon_{Ni})} + (1 - \beta)\right]^{1/3} + 1\right\} \quad (19)$$

This method of treating the influence of reduction is an over-simplified one. However, the effect on tortuosity is relatively small. Also, all data show that the effect of reduction is related to shrinkage. Therefore, a quantitative treatment should involve the densities and extent of reduction and Equation (19) does this.

Predictive Equation for $\delta(\phi,\beta)$

It is assumed that the effect of reduction is independent of sintering, or ϕ. Then $f(\beta) = \delta(\phi, \beta)/\delta(\phi, 0)$ or

$$\delta(\phi, \beta) = \delta(\phi, 0) f(\beta) \quad (20)$$

Substituting Equation (15) for $\delta(\phi, 0)$ gives

$$\delta(\phi, \beta) = g(\phi)\,\delta(0, 0)\,f(\beta) \quad (21)$$

$\delta(0, 0)$ refers to the tortuosity of unsintered and unreduced pellets and is given by Equation (13). Also, $f(\beta)$ is described by Equation (19). Hence, the final expression for δ is

$$\delta(\phi, \beta) = g(\phi)\left(\frac{1}{\epsilon_0}\right)\frac{1}{\sqrt{2}}\left\{(\sqrt{2} - 1)\left[\frac{0.78\,\rho_{NiO}\beta}{\rho_{Ni}(1 - \epsilon_{Ni})} + 1 - \beta\right]^{1/3} + 1\right\} \quad (22)$$

where ϵ_0 is the porosity of the pellet prior to sintering and reduction.

Before Equation (22) can be used as a predictive method ϵ_{Ni} must be known. Mercury porosimeter measurements for highly reduced pellets (19 and 20) showed very small volumes for pores less than 0.02 microns in diameter. Since intraparticle pores are likely to be much smaller (NiO particle size = 0.45 microns) the porosity of the nickel layer is expected to be low. Further the effect of ϵ_{Ni} values between 0 and 0.1 on δ calculated from Equation (22) is less than the accuracy of the experimental tortuosity factors. Hence, little error is expected in choosing $\epsilon_{Ni} = 0$.

Equation (22) expresses $\delta(\phi, \beta)$ in terms of the two variables β and ϵ, since ϕ is a function of ϵ from Equation (16). However, Equation (16) as is shows only the effect of ϕ on porosity. It cannot be used to obtain ϕ when reduction also occurs because porosity changes with extent of reduction. Instead of ϵ_0 it is necessary to use a porosity ϵ_B in Equation (16) such that the equation describes only the effect of ϕ on porosity. That is, ϵ_B is the porosity that would exist if no change in ϕ occurred during reduction. Then ϵ_B can be calculated from the effect of shrinkage on the porosity, that is, from ϵ_0 and β. From simple geometric considerations,* for spherical particles the relation $\epsilon_B = f(\epsilon_0, \beta)$ is

$$\frac{1 - \epsilon_B}{1 - \epsilon_0} = \frac{0.78\,\rho_{NiO}\beta}{\rho_{Ni}} + (1 - \beta) \quad (23)$$

After calculating ϵ_B from Equation (23), ϕ is estimated from

$$\epsilon = \epsilon_B(1 - \phi) \quad (24)$$

The end result is that Equation (22) can be used to predict δ for any degree of sintering and reduction from measured values of ϵ, ϵ_0, and β. No adjustable parameters are involved. The equation is limited to pellets prepared from nonporous particles. The procedure is as follows:

1. Estimate ϵ_B from ϵ_0 and β from Equation (23)
2. Determine ϕ from ϵ and Equation (24)
3. Obtain $g(\phi)$ from Figure 10
4. Calculate $\delta(\phi, \beta)$ from Equation (22).

* The original development of the factor $\sqrt{2}$ was based upon a model depicting pores as being randomly oriented in direction. However, the result is equivalent to assuming a single pore whose axis is at an angle of 45° with respect to the direction of diffusion.

* See footnote on page 671.

COMPARISON OF THEORY WITH EXPERIMENT

The solid lines in Figures 6 and 7 represent predictions from Equation (22). Figure 6 shows that the effect of sintering is well accounted for by the theory down to porosities as low as 0.1. In the region $0.1 < \epsilon < 0.44$, the extent of pore interconnections is dominant in determining the effect of sintering. For lower porosities, experimental δ are less than the predicted values. The effect of pore interconnections $g(\phi)$ was developed assuming an isotropic pore structure, which is probably less accurate at very low porosities. Also severe sintering could cause cracks to appear, although this was not evident from our observations. Cracks would have the effect of increased pore interconnections, giving lower tortuosity factors in agreement with the direction of the deviations. Pore-size changes during sintering were not considered in deriving $g(\phi)$. Figure 3 indicates that the mean pore radius ultimately decreases (Pellets 9, 10) with sintering, although for slightly sintered pellets $\bar{r}$ is nearly constant. Pore shrinkage would tend to make the predicted δ too low. Figure 6 also includes data for the effect of pelleting pressure (pellets 1, 2, 13), and here the RPM adequately represents the tortuosity factors.

The effect of reduction on highly sintered pellets is to reduce the tortuosity factor, as shown in the results for pellets 20 and 21 in Figure 7. According to the theory, this reduction results from an increase in pore interconnections as reduction proceeds. In this view shrinkage of the particles during reduction would cause the thin bridges of solid connecting sintered particles to collapse. As mentioned, the original, unreduced pellets from which pellets 20 and 21 were prepared had porosities of 0.09 and tortuosity factors of about 33. Comparison of the predicted and experimental points in Figure 7 for pellets 20 and 21 shows that this concept agrees well with the data.

Figure 7 also indicates that the tortuosity changes but little during reduction for an unsintered pellet (pellets 18 and 19). This is explained as the result of the effects of porosity and pore interconnections approximately balancing each other. The increase in porosity during reduction causes an increase in diffusion rate or a decrease in tortuosity. However, some sintering may occur at localized spots within the pellet during reduction. This decreases pore interconnections (increases ϕ) and increases δ. The resultant increase in tortuosity factor suggests that for the NiO case the sintering effect predominates. The predicted values for pellets 18 and 19 are slightly lower than the experimental ones but the trend with extent of reduction is adequately predicted.

CONCLUSIONS

Diffusion measurements for highly sintered pellets of NiO particles led to tortuosity factors of as high as 100 in comparison with values of 3 to 4 in most porous catalysts.

An approximate theory was developed for predicting the effects of sintering and chemical reduction on diffusion rates. The basis for the development is that sintering reduces pore interconnections and reduction causes the porosity and diffusion path length to change due to density changes. The random pore model fit diffusion data for unsintered and unreduced pellets. Hence, the RPM could be used as the foundation for deriving a predictive equation for the absolute value of the tortuosity factor at any condition of sintering and reduction. The resultant expression involves no adjustable parameters and requires for application the fractional reduction β, the porosity ϵ of the pellet, and the porosity ϵ_0 of the corresponding unsintered, unreduced pellet.

The theory agreed well with experimental results for pellets of NiO particles. Information is needed for other materials to test the generality of the development. Accounting for anisotropy in the pore structure, particularly at low porosities, for the effect of pore-size changes on the sintering effect, and for the level of sintering on the reduction effect, could lead to improved results.

NOTATION

C = concentration of diffusing component, g moles/cm^3
D = composite diffusivity in a straight capillary, defined by Equation (8)
D_e = approximate, effective diffusivity in a porous media, defined by Equation (2), cm^2/s
D_{AB} = bulk molecular diffusivity in binary mixture of A and B, cm^2/s
D_{KA} = Knudsen diffusivity of gas A, evaluated for the average pore radius $\bar{r}$, cm^2/s
$f(\beta)$ = effect of chemical reduction on tortuosity factor, defined by Equation (20)
$G(r)dr$ = distribution function for pore radii, defined by Equation (6), cm^3
$g(\phi)$ = effect of pore interconnections (sintering) on tortuosity factor, defined by Equation (15)
ΔL = pore length, cm
M = molecular weight, g/mole
m = number of particles in a pellet
n = number of pores; n_0 = total number of pores in an array
N = number of pores in the direction of diffusion in an array
N_A = diffusion flux of component A, g moles/cm^2 s
P = total pressure
R_g = gas constant
R = radius of partially reduced particle; R_0 = radius of unreduced particle, cm
r = pore radius; $\bar{r}$ = mean pore radius defined by Equation (4), cm
S_g = surface area of pores, defined by Equation (5), cm^2/g
T = temperature, °K
V = pore volume; V_t = total pore volume in pellet, cm^3/g
V_p = volume of pellet, cm^3
W = mass of pellet
y_A = mole fraction of gas A
z = distance coordinate in the direction of diffusion, cm

Greek Letters

α = $1 + N_B/N_A$
β = fraction of nickel oxide reduced to nickel
δ = tortuosity factor
ϵ = porosity of pellet; ϵ_0 = porosity of unsintered, unreduced pellet; ϵ_B = porosity that would exist if there were no change in ϕ during reduction; ϵ_{Ni} = porosity of layer of reduced nickel surrounding NiO particles
ρ = density, g/cm^3
ϕ = fraction of pores removed in an array

LITERATURE CITED

Bonis, L. J., and H. H. Hausner, *Proc. Symp. on Fundamental Phenomena in the Material Sciences*, p. 11-24, Plenum Press, New York (1964).

Calvelo, A., and R. E. Cunningham, "Kinetics of Gas-Solid Reactions. Influence of Surface Area and Effective Diffusivity Profiles," *J. Catalysis*, **17**, 1 (1970).

Evans, R. B., G. M. Watson, and E. A. Mason, "Flow and

Diffusion of Gases in Porous Media," *J. Chem. Phys.*, **46**, 3199 (1967).
Kim, K. K. "Effect of Sintering and Reduction on Diffusion in Nickel Oxide Pellets," Ph.D. dissertation, Univ. California, Davis (1973).
Krasuk, J. H., and J. M. Smith, "Kinetics of Reduction of Nickel Oxide with Carbon Oxide," *AIChE J.*, **18**, 506 (1972).
Kuczynski, G. C., A. N. Houton, and C. F. Gibbon, *Proc. Conf. on Sintering and Related Phenomena*, Sect. I, p. 1-233 and Sect. II, p. 245, 301, 345, Gordon and Breach, New York (1967).
Szekely, J., and J. W. Evans, "Studies in Gas-Solid Reactions: Part II. Study of Nickel Oxide Reduction with Hydrogen," *Metallurg. Trans.*, **2**, 1699 (1971).
———., "A Structural Model for Gas-Solid Reactions with a Moving Boundary," *Chem. Eng. Sci.*, **26**, 1901 (1971).
———., W. H. Ray, and Y. K. Chuang, "On the Optimum Temperature Progression for Irreversible Non-catalytic Gas-Solid Reactions," *Chem. Eng. Sci.*, **28**, 683 (1973).
Wakao, N., and J. M. Smith, "Diffusion in Catalyst Pellets," *Chem. Eng. Sci.*, **17**, 825 (1962).
Wicke, E., and R. Kallenbach, "Counter Diffusion Through Porous Pellets," *Kolloid. Z.*, **97**, 135 (1941).

Manuscript received January 7, 1974; revision received March 25 and accepted April 6, 1974.

Growth of Nickel Sulfate in a Laboratory-Scale Fluidized-Bed Crystallizer

Growth and dissolution rates of nickel sulfate α-hexahydrate were measured as functions of the concentration driving force in a laboratory-scale fluidized-bed crystallizer for the temperature range 35° to 50°C and the crystal size range 0.5 to 4.0 mm.

Dissolution rates at a given temperature and crystal size were first order in the concentration driving force. Growth rates were about one-quarter of dissolution rates and depended on a higher exponent (around 1.3) of the concentration driving force. This exponent was not significantly affected by variations in crystal size, but decreased as temperature increased. The apparent variation of growth rate itself with crystal size at constant temperature was slight. Growth rates were found to be insensitive to solids concentration.

V. ROGER PHILLIPS
and
NORMAN EPSTEIN

Department of Chemical Engineering
The University of British Columbia
Vancouver, B. C., Canada V6T 1W5

SCOPE

Laboratory-scale studies of fluidized-bed crystallization are of interest as aids to the design of full-scale crystallizers of the suspended-bed (Krystal) type. Measurements on crystal growth rates under conditions simulating those in industrial crystallizers, especially Krystal crystallizers, are still relatively scarce. Crystal growth rates determined under controlled conditions can also be used to test theories of the mechanism of crystallization. In this respect, dissolution rates determined under comparable conditions indicate the role of mass transfer in the overall growth process.

The α-hexahydrate crystallizes from solution at temperatures between 31.2° and 53.3°C. Although nickel sulfate has some commercial significance (being a byproduct of copper refining and being used mainly in electroplating, in the preparation of catalysts and as a fungicide), no previous measurements could be found on the rates of growth of any of its hydrates. In the present work, growth and dissolution rates of the α-hexahydrate were measured as functions of the concentration driving force in a laboratory-scale fluidized-bed crystallizer. The range of temperature studied (with a constant crystal size of 1 mm) was 35° to 50°C and the range of crystal size studied (with a constant temperature of 40°C) was 0.5 to 4.0 mm.

The apparatus is shown in Figure 1. Supersaturated solution at constant temperature is continuously circulated around a vertical rectangular circuit. The circulation rate and the concentration of the solution are known. In the Differential Method (for which the void fraction is about 0.998), a series of separate experiments is made at each temperature and crystal size, the supersaturation or undersaturation level being almost constant within each experiment but different between experiments. A small weight of seed crystals is used and the growth or dissolution rate is found via the change in weight of the crystals. In the Integral Method (for which the void fraction is about 0.80, close to industrial levels), supersaturation or undersaturation levels are permitted to fall by a large amount while being continuously monitored. A large weight of seed crystals is used and growth or dissolution rates are found from the rates of fall-off of solution supersaturation or undersaturation. This method allows growth or dissolution rates to be determined much more rapidly, but its use for growth studies is restricted to low supersaturations. In the present work this method was applied only to the growth of 1 mm crystals at 40°C.

These are believed to be the first growth rate measurements reported for nickel sulfate, a compound of some commercial significance. While it is realized that in the industrial crystallization of nickel sulfate, the feed solutions are not pure, it is suggested that the present measurements represent the asymptotic growth rates as impurity levels tend to zero.

V. R. Phillips is with the Department of Chemical Engineering, University College London, Torrington Place, London WC1E 7JE, England.